Carbon reduction powered by natural electrochemical gradients under submarine hydrothermal vent conditions

T. Altair[1,2], E. Dragoti[1], V. Sojo[3], Y. Li[4,5], S.E. McGlynn[4,5,6], D. Galante[7], H. Varela[2], R. Hudson[1]

AUTHOR ADDRESS. [1]College of the Atlantic, Bar Harbor, USA, [2] São Carlos Institute of Chemistry, University of São Paulo São Carlos, Brazil, [3] Institute for Comparative Genomics & Richard Gilder Graduate School, American Museum of Natural History, New York, USA, [4] Earth-Life Science Institute, Institute of Science Tokyo, Tokyo, Japan, [5] Center for Sustainable Resource Science, RIKEN, Saitama, Japan, [6] Blue Marble Space Institute of Science, Seattle, USA, [7] Institute of Geosciences, University of Sao Paulo, Sao Paulo, Brazil.

KEYWORDS: Emergence of life, Submarine Alkaline Vents, Alkaline hydrothermal vents, Iron Sulfides, Electrochemistry, Acetyl-CoA pathway.

ABSTRACT: Energy metabolism at the emergence of life has been the topic of intense theoretical and experimental study. Alkaline hydrothermal vents (AHVs) may have facilitated energy-transfer and carbon-fixation at life's emergence, via a primordial chemiosmotic mechanism. Specifically, pH separation across vent walls could have been the forerunner to pH separation across microbial membranes, with electron-conductive inorganic barriers containing [Ni-]FeS minerals mimicking the active sites of metalloenzymes in potentially ancient biological reductive acetyl-CoA Wood-Ljungdahl (WL) pathway, reverse Krebs and other metabolic pathways. We previously demonstrated pH gradient dependent reduction of CO_2 to formate by H_2 in AHV interface conditions. Here, we address the same problem of CO_2 reduction, however using a macroscale reactor that allowed us to use minerals synthesized via protocols analogous to the alkaline vent mount formation. This reactor also allowed us to probe more variables, and explore longer experimentation time-frames. Thus, this work aimed to investigate the effect of the different aspects of the gradient-rich hydrothermal-vent interface on the observed CO_2 electrochemical reduction- such as different minerals, temperature gradients, as well as the flow of electrons under passive vs. induced currents and potentials. Using experimental simulations and electrochemistry techniques, We detected two key steps of the WL pathway (CO_2 to formic acid, and the formation acetic acid) as well as reactions in the reverse Krebs cycle (fumarate to succinate). Both Ni in the mineral, and temperature as a property, were shown to affect the formation of formate. Extremely small currents were enough to efficiently carry out CO_2 reduction. This work develops benchmarks to electrochemically explore the model of protometabolisms in the vent-ocean interface and opens to future analyses on the catalytic or electrocatalytic properties of Fe-[Ni-]S minerals as precursors of metalloenzymes.

INTRODUCTION: The hydrothermal-vent interface of early submarine vent systems has long been proposed as a hatchery for the emergence of early bioenergetic processes.[1,2] This model is based on the mechanism of chemiosmosis, or vectorial electrochemistry,[3–5] which describes an energy conversion mechanism, universal in known modern cells. In that cell mechanism, exergonic and endergonic processes are coupled using natural electrochemical gradients, resulting from the pH and redox gradients, as drivers to chemical reactions, mediated by membrane-located molecular machines, or enzymes.[6] This energy conversion system is considered as universal and antique as the genetic code in known living systems.[7,8] In a model of early cell metabolism, a key step for emergence includes the reduction of the oceanic CO_2 by serpentinization-derived H_2 mediated by vent minerals, in a prebiotic analogy to the reductive acetyl Coenzyme A (also known as Wood-Ljunghdahl pathway; WL).[9,10] From this context, we investigate the first steps for the emergence of key metabolism for life. We focus here on models of prebiotic pathways based on the Wood-Ljungdahl (WL) pathway and on the reverse tricarboxylic acid (rTCA) cycle. Both are considered key protometabolism for the early phases of biochemical evolution involving Acetyl-CoA an highly-reactive and energy-rich molecule.[10–12]

In environments with alkaline vents, this model for the emergence of bioenergetics offers pH and electrochemical gradients as driving forces for proto-biological processes, facilitated by the interface between hydrothermal fluids and the primitive ocean (which we will refer to as early vent-ocean interface). Vent efflux of moderate temperature (~70ºC), moderate reducing potential and alkalinity (pH ~9), juxtaposed

with the cold, acidic oceanic fluids, percolate a labyrinth of micropores in the mineral precipitate (predominantly formed by carbonates) that mediate the interface.[13] The mechanism of catalysis proposed is by minerals composed of iron and sulfur (Fe-S minerals) or iron oxyhydroxides (green rusts)—both plausible on early Earth in the context of hydrothermal vents.[9,14,15] Clusters of Fe-S and iron oxides are considered precursors of important enzymes for carbon transduction and fixation processes, such as the case of the WL pathway.

The WL pathway depends, like other cellular processes, on a proton gradient for the reduction of CO_2 by molecular hydrogen using iron center proteins in the active site of enzymes working at the intersection of membranes, such as ferredoxin. Thioesters, such as Acetyl-CoA, are extremely important in prokaryotic metabolisms such as methanogens and acetogens, in transduction pathways without the participation of ATP or any other triphosphate.[16–18] Furthermore, CO_2 is a component of relative abundance in the primitive ocean, and H_2 is a product of serpentinization reaction.[19,20] Given the universality of the Acetyl-CoA pathway, such metabolism may have already existed in the Last Universal Common Ancestor (LUCA).[17,21,22] The initial and limiting step of this metabolism, the formation of formic acid from CO_2, was recently demonstrated in the laboratory in the absence of enzymes, using the mediation of metallic samples, and under hydrothermal conditions.[22]

The emphasized variant of the submarine alkaline vent theory (SAVT) has already guided experimental works that explored the proposed requisite mechanisms of early energy conversion.[23–26] Recently, We recently demonstrated CO_2 reduction to formate by H_2, which is the first and limiting step of WL pathway, using microfluidic setups under the conditions of the early vent-ocean interface.[27,28]

These microfluidc studies elucidated important aspects of a possible carbon-fixation mechanism hosted in the early hydrothermal-vent interface. Specifically, they suggest an indirect electrochemical coupling of the CO_2 reduction process with H_2 oxidation that occur on different sides of the inorganic barrier. Herein, to better probe the mechanism, we employ macroscale reactors in our examination not only for CO_2 reduction to formate, but also the first C-C bond forming step in the production of acetic acid. Thus, we aimed to simulate different conditions estimated to exist in a gradient-rich early alkaline vent scenario and investigate the effects of those variables on the limiting key steps of the Acetyl-CoA pathway using FeS minerals. The effect of the presence of Ni in the mineral structure, the thermal gradient and the occurrence of different passive and induced electrical currents were tested in order to better understand how those conditions might have contributed to CO_2 fixation at early hydrothermal-vent interfaces. Beyond CO_2 fixation, we also focused on other anabolic reactions in the reverse Krebs cycle (which in contemporary systems the WL pathway feeds into). Such reverse Krebs cycle reactions are also expected to have succeeded the WL pathway at the onset of life and it has previously been demonstrated in geologically plausible batch conditions.[29–31] We showcase reactions from the reverse Krebs cycle (fumarate reduction to succinate) by the indirect, gradient induced electroreduction in a separated cell reactor. Moreover, we also investigate the structure and composition of FeS minerals formed by co-precipitation used in a variety of microfluidic protocols.[28,32–35] Finally, the macroscale reactor used in this study enables electrochemical monitoring, allowing us to probe the electron-transfer mechanism for the redox reactions involving CO_2 and H_2 mediated by the mineral interface.

METHODS:

Materials and solutions preparation. All solutions were prepared with high purity water (Milli-Q system, 18.2 MΩ.cm) and with reagent grade chemicals. The main electrolytes used, the vent analog and ocean analog fluids, was based on works form literature (Table S1). [9,28,32] For saturation of solutions, CO_2 and H_2 gases (purity: 99.99%) were used.

Synthetic minerals preparation. For the synthesis of FeS and Ni-FeS, a co-precipitation method, also based on the literature,[9,28,32] was used. In this work, mineral-formation fluids (Table S1) were mixed in a 1:1 proportion to form the precipitates of Fe-S and Ni-Fe-S minerals. Then, the resulting suspension was separated by centrifugation and the precipitated mineral paste was used as an electron-conductive ink painted onto Fe electrodes.

Synthetic minerals analyses. The synthesized minerals were characterized via powder x-ray diffraction (p-XRD), and x-ray fluorescence (XRF).

Experimental setups. For experiments investigating the pH and redox gradient driven CO_2 reduction mediated by different minerals and the effect of thermal gradient, we used a two-chamber glass reactor with separated water jackets and capacity of 250 mL in each chamber (Figure S1). For simulating the vent-ocean interface, a vent analog fluid and an early ocean analog were used as electrolytes. Natural pyrite pieces or Fe pieces painted with a mineral ink were mediating the interface in contact of both fluids simultaneously. Moreover, an external electron-conductive wire connected both pieces immersed in the electrolytes. An ion-exchange membrane (Nafion 212), pretreated in 0.1 M NaOH, separated the two chambers for ionic equilibration during experiments.

For analyzing thermal-gradient effects, the two-chamber glass reactor was used, with separate temperature control for the two compartments (vent/ocean: 75˚C/75˚C; 75˚C/5.5˚C; 5.5˚C/5.5˚C).

In order to directly electrochemically monitor the system with a potentiostat, we used a smaller reactor with a shorter distance between electrodes, and thus less resistivity overall. This two chamber PTFE reactor had a 20-mL capacity and a magnetic stirrer in the ocean side (Figure S3). The same electrolytes, ion exchange membrane and minerals used with the large glass reactor were used here. For these experiments we

chose several fixed voltage (-0.5V and -2V), as well as an 'expected' current (10 nanoamperes; based on the resistivity of the system, and the potential difference) and a greater 10 microampere current.

In order to explore the capacity for the separated cell system to enable the reduction of other organics, we used a similar two-chamber PTFE reactor with a 20 mL capacity. On the vent side, we used the same alkaline vent efflux solution described above (with a hydrogen balloon), and on the ocean side, the electrolyte was KI, with fumarate as the reactant, and rather than CO_2 gas (we used a balloon of N_2 so as to eliminate the possibility for competing organic reductions.

For all the experiments described, the organic aqueous product analyzes were performed via proton nuclear magnetic resonance (^{1}H-NMR) and ^{13}C NMR.

RESULTS:

Synthetic minerals analyses. The process of bulk precipitation for mineral formation is estimated to be analogous to the one that occurs in hydrothermal vent system resulting in its typical porous inorganic barriers that form the vent mounts.[36–38] The XRD analyses of those minerals showed the typical profile from amorphous or nanocrystaline structures (see Supplementary material), likely due to the formation of several phases simultaneously. XRF (Fig. S4) suggests similar stoichiometric ratios of metal (Fe or Fe/Ni) to S present in the precipitated minerals.

Organics formation mediated by different [Ni-]FeS minerals. Screening of various minerals in the glass cell reactor indicated that FeS, Ni-FeS, and FeS_2 all produced short chain carboxylic acids in μM concentrations on the ocean side of the reactor at 25˚C (Table 1, entries 1-3), while none was detected on the vent side (Table 1, entry 4). This suggests that rather than gases or organic molecules passing between chambers, that there is instead an indirect electrochemical mechanism whereby H_2 is oxidized on the 'vent' side of the reactor, electrons pass through the mineral, and reduce organics on the 'ocean' side of the reactor. Single-pot blank reactions—[Ni-]FeS minerals with CO_2 gas (Table 1, entry 5), and no mineral with CO_2 and H_2 (Table 1, entry 6)—offered neither formic acid nor acetic acid. This suggests that under ambient temperature (~22-25°C) and anoxic condition the mineral cannot be significantly sacrificially oxidized as the source of electrons for CO_2 fixation, and nor can CO_2 & H_2 together effect such reactions in the absence of an electrocatalyst.

In general, Ni-FeS mineral mediating the vent-ocean interface resulted in roughly similar yields of formic acid, as occur to gas products shown in the work of Yamaguchi et al., (2014).[5] The same pattern was also detected to occur on acetic acid formation.

Effects of the thermal gradient. Adapting the reactor setup (Figure S1b), we screened the effect of temperature on both chambers. With both chambers at 75˚C, formic and acetic acid were observed in appreciable quantities (Table 2, entry 1), whereas when both chambers were cooled to 6˚C, none was detected (Table 2, entry 2). Under a temperature-gradient scenario similar to Hadean vent models, the yields for formic acid and acetic acid (Table 2, entry 3) nearly matched the all-hot tests. Coupled with the all hot (slightly higher organic formation) and all cold (no products detected) tests, the temperature gradient results suggest that higher temperatures on the vent side increase the rate of H_2 oxidation (the reaction cannot proceed with a 'cold' vent side). The ocean side can be either 'hot' or 'cold', and still produce significant short chain carboxylic acids. Perhaps the thermodynamic effect of temperature reduction on the ocean side is countered by kinetic advantage of increased concentrations of CO_2 at colder temperatures.

Current control and second protometabolic step. To simulate and investigate specific electrochemical conditions on the vent-ocean interface, experiments were performed in the

Table 1. Organics formed from different minerals mediating the early vent-ocean interface at different conditions after 24 h using two-chamber reactor as shown in Fig S1a.

Entry	Mineral	Ocean side gas, pH, T/˚C	Vent side gas, pH, T/˚C	Formic acid (μM)	Acetic acid (μM)
1	FeS_2[a]	CO_2, 5.7, 25	H_2, 11, 25	4.2	2.5
2	Ni-FeS[a]	CO_2, 5.7, 25	H_2, 11, 25	3.9	n.d.
3	FeS[a]	CO_2, 5.7, 25	H_2, 11, 25	n.d.	13
4	FeS[c]	CO_2, 5.7, 25	H_2, 11, 25	n.d.	n.d.
5	FeS[b]	[single cell] CO_2, 4, 25		n.d.	n.d.
6	--[b]	[single cell] CO_2+H_2 4, 25		n.d.	n.d.

[a]reaction conditions: Large glass reactor. ocean side fluid: $Na_2Si_3O_7$ 10 mM in deionized water (purged with CO_2). Vent side fluid: Na_2S 100 mM, K_2HPO_4 10 mM, $Na_2Si_3O_7$ 10 mM (purged with H_2). Reactor set up with a nafion membrane separating the two cells of the reactor, and single piece of mineral or mineral plated electrode placed between a glass joint which is connected to each sample compartment by a fluoroelastomer tube. *Sample taken from 'ocean side' of reactor*
[b]blank reactions: This reaction was performed in a single compartment (not the separated cell used for electrochemical reactions).
[c]Sample taken from vent side rather than ocean side. Otherwise, same as [a]conditions
n.d. : None detected

Table 2. Organics formed after 18h in simulated early vent-ocean interface under thermal-gradient condition using two-chamber reactor as shown in Fig S1b.

Entry	Mineral	Ocean side gas, pH, T/°C	Vent side gas, pH, T/°C	Formic acid (μM)	Acetic acid (μM)
1	Ni-FeS	CO_2, 5.7, 75	H_2, 11, 75	815.8	33.54
2	Ni-FeS	CO_2, 5.7, 6	H_2, 11, 6	n.d.	n.d.
3	Ni-FeS	CO_2, 5.7, 6	H_2, 11, 75	735.9	11.15
n.d. : None detected					

range of conditions that is expected to exist in natural scenarios. A series of potentiostat-induced experiments were conducted under two conditions under fixated current (Table 3): -10 nA (nanoamp), and -10 μA (microamp). The magnitude of nanoamp was estimated to be the same of the spontaneous-condition experiment (Fig S2b). We also tested two conditions under fixated voltage: -500 mV and -2.0 V (Table 4). Hundreds of millivolts is a range that is also detected on natural hydrothermal systems and is estimated to have existed in early hydrothermal scenarios.[39,40] All the referred conditions were set considering the mineral in the ocean side as the working electrode.

Ni-FeS showed higher organic product formation and overall faradaic efficiency for CO_2 reduction at same electrochemical conditions than FeS (Figures S4 and S5). We also detected that under nanoamp current, the faradaic efficiencies were much higher for the organic production, mainly for Ni-FeS. That indicates that Ni atoms enhanced the interaction of mackinawite with CO_2 for its electrochemically-induced reduction, as shown in other works,[41,42] and how specific currents, not necessarily the higher ones, may result in better efficiencies. For acetic acid formation, Ni-FeS shows a higher performance on mediating its formation. However, under condition of a fixed voltage of -500 mV (Table 4, entries 1 and 3), we see a different pattern, where FeS shows higher capacity to form formic and acetic acid. That altered pattern was acetic acid. Moreover, the experimentation here was performed in a specific type of reactor that was designed to simulate the vent-ocean interfacial electrochemical conditions and the long period of residence for the experiments may also be the reason for the detection of acetic acid. Besides that, different phases show more stability under different potential, and some of those may prevail after the 12 hours of experiments, which can explain the different pattern observed under – 500 mV.

Notably, small amounts of organics were detected in the experiment performed in thermodynamically spontaneous conditions under no external electrochemical induction (Table 3, entries 5 and 6). In this experiment, two mineral-coated iron pieces are directly connected by an electron-conductive wire, without the mediation of the potentiostat (Figure S2b), thus only pH and redox gradients are acting. The fact that the formic acid and acetic acid yields in these spontaneous conditions are closest to those with an applied nanoamp current, suggests that in this passive system, a nanoamp current may be all that is passing through the mineral mediators.

Fumarate reduction to succinate. Beyond CO_2 reduction, we were interested in the ability of the separated cell reactor to facilitate other metabolic reductions (Table 5). We therefore explored the reduction of fumarate to succinate under similar conditions as those used above for CO_2 fixation.

Blank reactions (where the mineral electrodes in the separate compartments were not connected) did not result in any

Table 3. Results of organic formation after 12h from current-induced experiments using the PTFE two-chamber reactor setup (Fig. S2) under room temperature.

Entry	Mineral	Current induced	Ocean side gas, pH, T/°C	Vent side gas, pH, T/°C	Formic acid		Acetic acid	
					Concentration (μM)	Faradaic efficiency	Concentration (μM)	Faradaic efficiency
1	FeS	10 nA	CO_2, 5.7, 25	H_2, 11, 25	5.56	20.67%	6.40	8.8%
2	FeS	10 μA	CO_2, 5.7, 25	H_2, 11, 25	n.d.	0%	4.86	0.005%
3	Ni-FeS	10 nA	CO_2, 5.7, 25	H_2, 11, 25	8.84	32.77%	43.23	29.05%
4	Ni-FeS	10 μA	CO_2, 5.7, 25	H_2, 11, 25	12.70	0.05%	12.41	0.012%
5	FeS[a]	-	CO_2, 5.7, 25	H_2, 11, 25	1.26	-	0.43	-
6	Ni-FeS[a]	-	CO_2, 5.7, 25	H_2, 11, 25	34.37	-	11.22	-
[a]Spontaneous system. Minerals were connected by an electron-conductive wire (Fig S2b) n.d. : None detected								

Table 4. Results of organic formation after 12h from voltage-induced experiments using PTFE reactor setup (Fig. S2) under room temperature.

Entry	Mineral	Voltage induced (V)	Ocean side gas, pH, T/°C	Vent side gas, pH, T/°C	Formic acid		Acetic acid	
					Concentration (μM)	Faradaic efficiency	Concentration (μM)	Faradaic efficiency
1	FeS	-0.5	CO_2, 5.7, 25	H_2, 11, 25	667.54	0.74%	17.32	0.005%
2	FeS	-2.0	CO_2, 5.7, 25	H_2, 11, 25	834.02	0.20%	30.77	0.0019%
3	Ni-FeS	-0.5	CO_2, 5.7, 25	H_2, 11, 25	762.31	0.29%	19.50	0.0019%
4	Ni-FeS	-2.0	CO_2, 5.7, 25	H_2, 11, 25	558.49	0.10%	30.96	0.0022%

observed succinate product. Likewise, reactions conducted with a weak vent electrolyte solution formed little to no product. FeS, FeS_2 and Ni-FeS facilitated the reaction in moderate yield (5-17%), whereas a bare Fe electrode produced very little succinate (1%). The lack of reactivity without electrodes connected indicates that sacrificial oxidation[43] of the mineral in the ocean side is not reducing enough to drive the conversion of fumarate to succinate in that ocean chamber; instead fumarate reduction must be coupled to H_2 oxidation on the vent side (so without an electrical connection between these chambers, this reduction cannot occur). Additionally, the lack of reactivity with a dilute vent electrolyte suggests the role of sulfide as an important reducing agent in addition to H_2 gas as well as the role of the electrolyte in charge mobility through the aqueous medium. The yields for fumarate reduction with the full strength electrolyte (5-17%) are on par with those demonstrated in a single-pot reaction for Fe/Ni minerals & metals,[25] although this is the first such demonstrated case of fumarate reduction where the H_2 provided is not oxidized in the same chamber, but instead it's oxidation is electrochemically coupled across a mineral electrocatalyst.

Table 5. Fumarate reduction to succinate in a macroscale simulated hydrothermal vent[a]

Mineral	Blank[b]	weak vent electrolyte[c]	Strong vent electrolyte
FeS	0%	0.5%	5%
FeS_2	0%	0%	8%
Ni-FeS	0%	0%	17%
Fe	0%	0.6%	1%

[a] reaction conditions: Small PTFE reactor. reactor set up with two separate mineral-painted electrodes placed in the separate chambers and connected by a wire. A Nafion membrane separates the sides. Ocean side fluid: fumarate (1 mmol), KI (10 mM) in deionized water (purged with N_2); temperature = 25 ˚C. Vent side fluid: Na_2S 100 mM, K_2HPO_4 10 mM, $Na_2Si_3O_7$ 10 mM (purged with H_2), temperature = 25 ˚C. Sample taken from the ocean side.
[b] reaction conditions: Same as ([a]), but electrodes in separate chambers not connected by a wire
[c] reaction conditions: Same as ([a]), but vent-side electrolyte fluid is 1000x weaker. Na_2S (0.1 mM), K_2HPO_4 (0.01 mM), $Na_2Si_3O_7$ (0.01 mM)

DISCUSSION:

The effect of thermal gradient for the energy protometabolism at early hydrothermal systems. Thermal gradients are known to exist in modern cellular systems, besides that is still under debate how crucial they are or their exact function for life. There is the example of the mitochondrial membrane where a 10˚C-gradient was detected.[44,45] Under interface conditions, the thermal gradient results in electrochemical potential, the well-known Seebeck effect/voltage. The potential generated from that effect is usually considered irrelevant, as it generally ranges from μV to hundredths of mV per Kelvin. On the other hand, thermodynamic and kinetic parameters of chemical reactions hosted in an interface region may be also considerably affected by temperature gradients. In the vent-ocean interface as modeled in the SAVT and evidenced by experimental works, there are reactions that are coupled on both sides of that interface and those can be independently affected by the local temperature on each side of the interface. The two reactions are represented below:

$$k\ CO_2(aq) + n(H^+ + e^-) \rightleftarrows P + m\ H_2O\ (l)$$

{P= HCOOH, CH_3COOH, HCHO}

$$H_2(aq) + 2\ OH^-(aq) \rightleftarrows 2\ H_2O\ (l) + 2\ e^-$$

In the early vent-ocean interface, both reactions are coupled and mediated by an inorganic electron-conductive [Ni-]FeS mineral. Figure 1 shows the result of an analytical model inspired by the works of Herschy et al.[9] and Ooka et al.[25] adapted to the context of the early vent-ocean interface. Based on that result, it is clear that thermodynamics becomes more favorable when there is a higher temperature gradient, as it increases the potential of both coupled reactions.

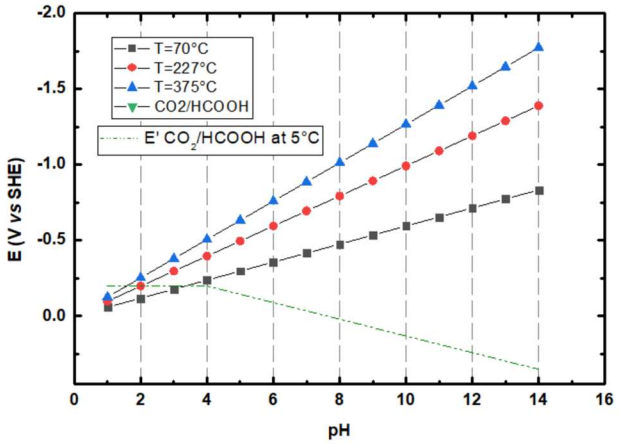

Figure 1. Equilibrium potentials for H_2 oxidation reaction (triangles, circles, and squares) at different temperatures based on different geological environments. The reference of the potentials calculated is the standard hydrogen electrode (SHE) Considering T=70°C detected in fluids of Lost City Hydrothermal Fields (LCHF)[46] and the natural radioactive environment in Witwatersrand basin,[47] T=227°C for the Okinawa Trough hydrothermal field,[25] and T=375°C for the Rainbow hydrothermal vent.[19] The potential required for reduction of CO_2 to HCOOH is shown (dashed line) by varying the pH and at the temperature of 5.5ºC, based on the work of Kortlever et al.[48]

The model that resulted in figure 1 illustrates the overall thermodynamic advantage that the thermal gradient may promote. On the other hand, there is evidence of the vent-ocean interface kinetics from the results of the all-cool and all-hot experiments. While, under low temperatures, H_2 and CO_2 gases are expected to be more soluble and the high concentration can increase the thermodynamic parameters, however, it can also decrease the reaction rates. Nevertheless, the reaction rates are expected to increase at higher temperatures, although the gas concentrations decrease. Thus, the organic formation detected under the all-hot conditions in higher concentration even compared to the experiments under thermal-gradient conditions and the fact that there were no organics under "all-cool"

conditions leads us to the conclusion that the kinetic control should prevail in the modeled system.

Outcomes for the emergence of life model in early AHV systems. Modern hydrothermal systems show natural electrical current and local reducing condition on its surface that also shows different potential and current at different regions.[39,40,49] Models of early alkaline hydrothermal systems also showed how electrochemical parameters might be sensitive to the early ocean local composition and consequently to the mineral barrier composition.[50] Here, we demonstrated how the Ni-FeS mineral formation condition in the alkaline hydrothermal systems results in a mixture of phases that cannot be easily identified. Under different surface potentials, [Ni-]FeS minerals can also change their prevailing phases, as shown in recent experimental works, which may promote the formation of a metal phase.[1151–53]

The gradient-rich along with the diversity of phases in the vent-ocean interface may be a key factor that makes the AHV scenario into a hatchery for life on early Earth, as envisioned in several works.[12,54–56] As concluded from the discovery of lamellar distribution of minerals in black smokers, with the inner layer dominated with chalcopyrite contacting hydrothermal fluid while the outside layer dominated with Pyrite (FeS_2) and sphalerite (Zn, Fe)S, and contacting the sea water. Inside that structure, the mineral layers are composed of pyrrhotite (FeS), pyrite and sphalerite. Such example of gradient structure is expected to affect the catalytic property at that submarine vent scenario.[57]

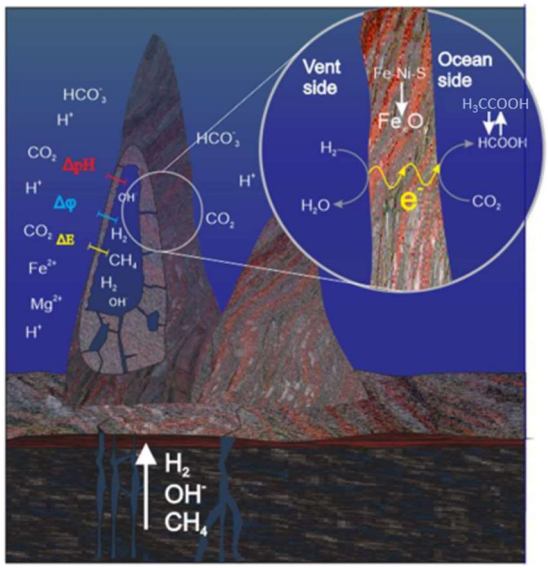

Figure 2. Sketch of the free-energy transfer mechanism from natural gradients on the early vent-ocean interface to drive the energy protometabolism, a candidate seed to the chemiosmosis' emergence on early Earth. It is represented the different gradients in the vent-ocean interface: the pH (ΔpH), redox ($\Delta\varphi$) and the resulting potential gradient (ΔE). The Ni-FeS-rich barrier mediates the electron-transfer mechanism coupling the H_2 oxidation and the CO_2 reduction in a WL-like protometabolism where two steps are occurring in the vent-ocean interface.

As shown here, after a period of hours, both formic acid and acetic acid are present in detectable concentrations under vent-ocean interface conditions. This indicates the possibility that at least two protometabolic steps could occur in the early vent-ocean interface, as illustrated in Figure 2. The variation of electrochemical conditions expected to exist on early hydrothermal systems, summed with the variation of Ni-FeS mineral phases does not compromise the occurrence of those protometabolic steps, but seems to only affect the accumulation of formic acid, probably due to the kinetics of the first step.

Moreover, we can expect that another factor can change the production of formic acid in that interface: the thermal insulation of the inorganic barrier. As shown here, warmer temperature on both sides of the vent-ocean interface contributes to higher rates of the CO_2 electrochemical reduction. This condition is expected to occur when thermal insulation is low enough, which can occur in regions of the vent system with thin barriers or closer to regions where serpentinization is occurring. On the other hand, on distant regions or where there is low serpentinization activity, thus cooler temperatures, very little CO_2 reduction can be expected, despite the presence of natural electrochemical gradients. In cases of high thermal insulation of the mineral, a temperature gradient (hot vent/cool ocean) is nearly as effective as the all-hot scenario.

Life thrives on harnessing efficiencies. While higher overall product formation can be seen at higher currents (10 microamperes), excellent faradaic efficiencies can be achieved with an approximation of the passive/expected current (10 nanoamperes). Herein, we demonstrated that a very small current can be extremely efficient for CO_2 reduction.

CONCLUSIONS:

This investigation into mineral facilitated electroreduction of CO_2 suggests conditions where reactions from a protometabolic Wood-Lyunghal pathway may be viable. Formic acid and acetic acid can be generated in μM quantities by the passive flow of electrons following geologically plausible pH and redox gradients established at hydrothermal vents. Additional downstream anabolic reactions (such as the conversion of fumarate to succinate) can also be carried out in the simulated hydrothermal vent. Higher temperatures lead to better conversion of CO_2 to formic acid, although the reaction can still proceed under a temperature gradient analogous to extant biological systems and similar to that expected for Hadean ocean vents. Extremely small currents (nanoamps) are enough with pH and redox gradients to efficiently enable CO_2 reduction. These results support the SAVT model while narrowing the search for optimal conditions for important protometabolic steps for a potential emergence of life. Our results also suggest that a variety of mineral mediators in the presence of a gradient-rich vent environment can induce two electrochemically-mediated metabolic steps for energy conversion and carbon fixation in the absence of enzymes at the interface of alkaline hydrothermal systems.

ASSOCIATED CONTENT

Supporting Information

XRF scans, pXRD patterns, ICP results, and NMR spectra are included in the Supporting Information. Detailed experimental procedures and reagents along with reactor schematics are included as well. The Supporting Information is available free of charge on the ACS Publications website.

AUTHOR INFORMATION

Corresponding Author

* (Word Style "FA_Corresponding_Author_Footnote"). Give contact information for the author(s) to whom correspondence should be addressed.

Present Addresses

†If an author's address is different than the one given in the affiliation line, this information may be included here.

Author Contributions

The manuscript was written through contributions of all authors. / All authors have given approval to the final version of the manuscript. / ‡These authors contributed equally. (match statement to author names with a symbol)

Funding Sources

Any funds used to support the research of the manuscript should be placed here (per journal style).

Notes

Any additional relevant notes should be placed here.

ACKNOWLEDGMENT

We thank the Maine Space Grant Consortium for financial support (SG-24-23: Hudson; SG-19-14 & SG-20-19 & EP-21-06 & EP-23-01: R.H., V.S.; EP-24-03: R.H., T.A., V.S.). R.H. acknowledges support from the JSPS (JSPS) (FY2016-PE-16047). The research reported in this paper was supported by an Institutional Development Award from the National Institute of General Medical Sciences of the NIH (P20GM103423). This study was also financed, in part, by the São Paulo Research Foundation (FAPESP), Brazil. Process Numbers 2018/12491-2 and 2020/13310-1. V.S. acknowledges support from the JSPS (FY2016-PE-16721), the European Molecular Biology Organization (ALTF-1455-2015), the Institute for Advanced Study in Berlin, and the Gerstner Family Foundation. SEM acknowledges JSPS KAKENHI grant number JP22K18278. DG acknowledges Sao Paulo Research Foundation, grant 2021/05083-8. HV acknowledges Conselho Nacional de Desenvolvimento Científico e Tecnológico (CNPq) for financial support (#140644/2020-2), and FAPESP for financial support (#2019/22183-6).

ABBREVIATIONS

WL, Wood-Lyungdahl; NMR, Nuclear Magnetic Resonance; SAVT, Subamarine Alkaline Vent Theory; XRD, X-ray diffraction; XRF, X-ray fluorescence; ICP, inductively coupled plasma;

REFERENCES

(1) Russell, M. J. A Self-Sustaining Serpentinization Mega-Engine Feeds the Fougerite Nanoengines Implicated in the Emergence of Guided Metabolism. *Front. Microbiol.* **2023**, *14* (May), 1–19. https://doi.org/10.3389/fmicb.2023.1145915.

(2) Schoepp-Cothenet, B.; Van Lis, R.; Atteia, A.; Baymann, F.; Capowiez, L.; Ducluzeau, A. L.; Duval, S.; Ten Brink, F.; Russell, M. J.; Nitschke, W. On the Universal Core of Bioenergetics. *Biochim. Biophys. Acta - Bioenerg.* **2013**, *1827* (2), 79–93. https://doi.org/10.1016/j.bbabio.2012.09.005.

(3) Lane, N.; Allen, J. F.; Martin, W. How Did LUCA Make a Living? Chemiosmosis in the Origin of Life. *BioEssays* **2010**, *32* (4), 271–280. https://doi.org/10.1002/bies.200900131.

(4) Mitchell, P. Vectorial Chemistry and the Molecular Mechanics of Chemiosmotic Coupling: Power Transmission by Proticity. *Biochem. Soc. Trans.* **1976**, *4* (3), 399–430. https://doi.org/10.1042/bst0040399.

(5) Yamaguchi, A.; Yamamoto, M.; Takai, K.; Ishii, T.; Hashimoto, K.; Nakamura, R. Electrochemical CO2 Reduction by Ni-Containing Iron Sulfides: How Is CO2 Electrochemically Reduced at Bisulfide-Bearing Deep-Sea Hydrothermal Precipitates? *Electrochim. Acta* **2014**, *141*, 311–318. https://doi.org/10.1016/j.electacta.2014.07.078.

(6) Simon, J.; van Spanning, R. J. M.; Richardson, D. J. The Organisation of Proton Motive and Non-Proton Motive Redox Loops in Prokaryotic Respiratory Systems. *Biochim. Biophys. Acta - Bioenerg.* **2008**, *1777* (12), 1480–1490. https://doi.org/10.1016/j.bbabio.2008.09.008.

(7) Lane, N. Proton Gradients at the Origin of Life. *BioEssays* **2017**, *39* (6), 1600217. https://doi.org/10.1002/bies.201600217.

(8) Orgel, L. E. Are You Serious, Dr Mitchell? *Nature* **1999**, *402* (6757), 17. https://doi.org/10.1038/46903.

(9) Herschy, B.; Whicher, A.; Camprubi, E.; Watson, C.; Dartnell, L.; Ward, J.; Evans, J. R. G.; Lane, N. An Origin-of-Life Reactor to Simulate Alkaline Hydrothermal Vents. *J. Mol. Evol.* **2014**, *79* (5–6), 213–227. https://doi.org/10.1007/s00239-014-9658-4.

(10) Russell, M. J.; Martin, W. The Rocky Roots of the Acetyl-CoA Pathway. *Trends Biochem. Sci.* **2004**, *29* (7), 358–363. https://doi.org/10.1016/j.tibs.2004.05.007.

(11) Kitadai, N.; Nakamura, R.; Yamamoto, M.; Okada, S.; Nakano, Y.; Takahashi, Y.; Takai, K.; Oono, Y. Thioester Synthesis through Geoelectrochemical. No. 2021. https://doi.org/10.1038/s42004-021-00475-5.

(12) Martin, W.; Russell, M. J. On the Origin of

Biochemistry at an Alkaline Hydrothermal Vent. **2007**, No. November 2006, 1887–1925. https://doi.org/10.1098/rstb.2006.1881.

(13) Kelley, D. S. A Serpentinite-Hosted Ecosystem: The Lost City Hydrothermal Field. *Science (80-.).* **2005**, *307* (5714), 1428–1434. https://doi.org/10.1126/science.1102556.

(14) Nitschke, W.; Russell, M. J. Beating the Acetyl Coenzyme A-Pathway to the Origin of Life. *Philos. Trans. R. Soc. B Biol. Sci.* **2013**, *368* (1622). https://doi.org/10.1098/rstb.2012.0258.

(15) Sojo, V.; Herschy, B.; Whicher, A.; Camprubí, E.; Lane, N. The Origin of Life in Alkaline Hydrothermal Vents. *Astrobiology* **2016**, *16* (2), 181–197. https://doi.org/10.1089/ast.2015.1406.

(16) Fuchs, G. *Alternative Pathways of Carbon Dioxide Fixation: Insights into the Early Evolution of Life?*; 2011; Vol. 65. https://doi.org/10.1146/annurev-micro-090110-102801.

(17) Lane, N.; Martin, W. The Energetics of Genome Complexity. *Nature* **2010**, *467* (7318), 929–934. https://doi.org/10.1038/nature09486.

(18) Russell, M. J.; Nitschke, W.; Branscomb, E. The Inevitable Journey to Being. *Philos. Trans. R. Soc. B Biol. Sci.* **2013**, *368* (1622). https://doi.org/10.1098/rstb.2012.0254.

(19) Lowell, R. P.; Rona, P. A. Seafloor Hydrothermal Systems Driven by the Serpentinization of Peridotite. *Geophys. Res. Lett.* **2002**, *29* (11), 26-1-26–4. https://doi.org/10.1029/2001GL014411.

(20) Kelley, D. S.; Karson, J. A.; Früh-Green, G. L.; Yoerger, D. R.; Shank, T. M.; Butterfield, D. A.; Hayes, J. M.; Schrenk, M. O.; Olson, E. J.; Proskurowski, G.; Jakuba, M.; Bradley, A. S.; Larson, B.; Ludwig, K.; Glickson, D.; Buckman, K.; Bradley, A. S.; Brazelton, W. J.; Roe, K.; Elend, M. J.; Delacour, A.; Bernasconi, S. M.; Lilley, M. D.; Baross, J. A.; Summons, R. E.; Sylva, S. P. A Serpentinite-Hosted Ecosystem: The Lost City Hydrothermal Field. *Science (80-.).* **2005**, *307* (5714), 1428–1434. https://doi.org/10.1126/science.1102556.

(21) Ducluzeau, A. L.; Schoepp-Cothenet, B.; Baymann, F.; Russell, M. J.; Nitschke, W. Free Energy Conversion in the LUCA: Quo Vadis? *Biochim. Biophys. Acta - Bioenerg.* **2014**, *1837* (7), 982–988. https://doi.org/10.1016/j.bbabio.2013.12.005.

(22) Muchowska, K. B.; Varma, S. J.; Moran, J. Synthesis and Breakdown of Universal Metabolic Precursors Promoted by Iron. *Nature* **2019**, *569* (7754), 104–107. https://doi.org/10.1038/s41586-019-1151-1.

(23) Yamaguchi, A.; Arai, K.; Aisnada, A. N. El; Lee, J.-E.; Kitadai, N.; Nakamura, R.; Miyauchi, M. Multi-Regression Analysis of CO 2 Electroreduction Activities on Metal Sulfides . *J. Phys. Chem. C* **2022**. https://doi.org/10.1021/acs.jpcc.1c08993.

(24) Möller, F. M.; Kriegel, F.; Kieß, M.; Sojo, V.; Braun, D.; Mçller, F. M.; Kriegel, F.; Kieß, M.; Sojo, V.; Braun, D.; Möller, F. M.; Kriegel, F.; Kieß, M.; Sojo, V.; Braun, D. Steep PH Gradients and Directed Colloid Transport in a Microfluidic Alkaline Hydrothermal Pore. *Angew. Chemie* **2017**, *129* (9), 2380–2384. https://doi.org/10.1002/ange.201610781.

(25) Ooka, H.; McGlynn, S. E.; Nakamura, R. Electrochemistry at Deep-Sea Hydrothermal Vents: Utilization of the Thermodynamic Driving Force towards the Autotrophic Origin of Life. *ChemElectroChem* **2019**, *6* (5), 1316–1323. https://doi.org/10.1002/celc.201801432.

(26) Altair, T.; Borges, L. G. F.; Galante, D.; Varela, H. Experimental Approaches for Testing the Hypothesis of the Emergence of Life at Submarine Alkaline Vents. *Life* **2021**, *11* (8), 1–27. https://doi.org/10.3390/life11080777.

(27) Hudson, R.; de Graaf, R.; Rodin, M. S.; Ohno, A.; Lane, N.; McGlynn, S.; Yamada, Y.; Nakamura, R.; Barge, L.; Braun, D.; Sojo, V. CO 2 Reduction Driven by a PH Gradient. **2020**. https://doi.org/10.1101/2020.03.02.973982.

(28) Sojo, V.; Ohno, A.; McGlynn, S. E.; Yamada, Y. M. A.; Nakamura, R. Microfluidic Reactors for Carbon Fixation under Ambient-Pressure Alkaline-Hydrothermal-Vent Conditions. *Life* **2019**, *9* (1). https://doi.org/10.3390/life9010016.

(29) Rauscher, S. A.; Moran, J. Hydrogen Drives Part of the Reverse Krebs Cycle under Metal or Meteorite Catalysis. *Angew. Chemie Int. Ed.* **2022**, *61* (51). https://doi.org/10.1002/anie.202212932.

(30) WACHTERSHAUSER, G.; Tal. Before Enzymes and Templates: Theory of Surface Metabolism. **1988**, *52* (4), 452–484.

(31) Russell, M. J.; Hall, A. J. The Emergence of Life from Iron Monosulphide Bubbles at a Submarine Hydrothermal Redox and PH Front. *J. Geol. Soc. London.* **1997**, *154* (3), 377–402. https://doi.org/10.1144/gsjgs.154.3.0377.

(32) Hudson, R.; de Graaf, R.; Strandoo Rodin, M.; Ohno, A.; Lane, N.; McGlynn, S. E.; Yamada, Y. M. A.; Nakamura, R.; Barge, L. M.; Braun, D.; Sojo, V. CO 2 Reduction Driven by a PH Gradient. *Proc. Natl. Acad. Sci.* **2020**, *117* (37), 22873–22879. https://doi.org/10.1073/pnas.2002659117.

(33) Wang, Q.; Barge, L. M.; Steinbock, O. Microfluidic Production of Pyrophosphate Catalyzed by Mineral Membranes with Steep PH Gradients. *Chem. - A Eur. J.* **2019**, *25* (18), 4732–4739. https://doi.org/10.1002/chem.201805950.

(34) Vasiliadou, R.; Dimov, N.; Szita, N.; Jordan, S. F.; Lane, N.; Lane, N. Possible Mechanisms of CO 2 Reduction by H 2 via Prebiotic Vectorial Electrochemistry. **2019**.

(35) Jackson, J. B. The “Origin-of-Life Reactor” and

Reduction of CO2 by H2 in Inorganic Precipitates. *J. Mol. Evol.* **2017**, *85* (1–2), 1–7. https://doi.org/10.1007/s00239-017-9805-9.

(36) Mielke, R. E.; Robinson, K. J.; White, L. M.; Mcglynn, S. E.; Mceachern, K.; Bhartia, R.; Kanik, I.; Russell, M. J. Iron-Sulfide-Bearing Chimneys as Potential Catalytic Energy Traps at Life ' s Emergence. **2011**, *11* (10). https://doi.org/10.1089/ast.2011.0667.

(37) Russell, M. J.; Daniel, R. M.; Hall, A. J.; Sherringham, J. A. A Hydrothermally Precipitated Catalytic Iron Sulphide Membrane as a First Step toward Life. *J. Mol. Evol.* **1994**, *39* (3), 231–243. https://doi.org/10.1007/BF00160147.

(38) Lee, H.-E.; Okumura, T.; Ooka, H.; Adachi, K.; Hikima, T.; Hirata, K.; Kawano, Y.; Matsuura, H.; Yamamoto, M.; Yamamoto, M.; Yamaguchi, A.; Lee, J.-E.; Nam, K. T.; Ohara, Y.; Hashizume, D.; Mcglynn, S. E.; Nakamura, R. Title Osmotic Energy Conversion in Deep-Sea Hydrothermal Vents.

(39) Nakamura, R.; Takashima, T.; Kato, S.; Takai, K.; Yamamoto, M.; Hashimoto, K. Electrical Current Generation across a Black Smoker Chimney. *Angew. Chemie - Int. Ed.* **2010**, *49* (42), 7692–7694. https://doi.org/10.1002/anie.201003311.

(40) Yamamoto, M.; Nakamura, R.; Kasaya, T.; Kumagai, H.; Suzuki, K.; Takai, K. Spontaneous and Widespread Electricity Generation in Natural Deep-Sea Hydrothermal Fields. *Angew. Chemie - Int. Ed.* **2017**, *56* (21), 5725–5728. https://doi.org/10.1002/anie.201701768.

(41) Kwon, K. D.; Refson, K.; Sposito, G. Transition Metal Incorporation into Mackinawite (Tetragonal FeS). *Am. Mineral.* **2015**, *100* (7), 1509–1517. https://doi.org/10.2138/am-2015-5211ccbyncnd.

(42) Wilkin, R. T.; Beak, D. G. Uptake of Nickel by Synthetic Mackinawite. *Chem. Geol.* **2017**, *462* (May), 15–29. https://doi.org/10.1016/j.chemgeo.2017.04.023.

(43) Garibello, C. F.; Simonov, A. N.; Eldridge, D. S.; Malherbe, F.; Hocking, R. K. Redox Properties of Iron Sulfides: Direct versus Catalytic Reduction and Implications for Catalyst Design. *ChemCatChem* **2022**, *14* (12). https://doi.org/10.1002/cctc.202200270.

(44) Chrétien, D.; Bénit, P.; Ha, H.-H.; Keipert, S.; El-Khoury, R.; Chang, Y.-T.; Jastroch, M.; Jacobs, H. T.; Rustin, P.; Rak, M. Mitochondria Are Physiologically Maintained at Close to 50 °C. *PLOS Biol.* **2018**, *16* (1), e2003992. https://doi.org/10.1371/journal.pbio.2003992.

(45) Knapp, B. D.; Huang, K. C. The Effects of Temperature on Cellular Physiology. *Annu. Rev. Biophys.* **2022**, *51*, 499–526. https://doi.org/10.1146/annurev-biophys-112221-074832.

(46) Kelley, D. S.; Karson, J. A.; Blackman, D. K.; Früh-Green, G. L.; Butterfield, D. A.; Lilley, M. D.; Olson, E. J.; Schrenk, M. O.; Roe, K. K.; Lebon, G. T.; Rivizzigno, P. An Off-Axis Hydrothermal Vent Field near the Mid-Atlantic Ridge at 30° N. *Nature* **2001**, *412* (6843), 145–149. https://doi.org/10.1038/35084000.

(47) Altair, T.; Sartori, L. M.; Rodrigues, F.; de Avellar, M. G. B.; Galante, D. Natural Radioactive Environments as Sources of Local Disequilibrium for the Emergence of Life. *Astrobiology* **2020**, *20* (12), 1489–1497. https://doi.org/10.1089/ast.2019.2133.

(48) Kortlever, R.; Shen, J.; Schouten, K. J. P.; Calle-Vallejo, F.; Koper, M. T. M. Catalysts and Reaction Pathways for the Electrochemical Reduction of Carbon Dioxide. *J. Phys. Chem. Lett.* **2015**, *6* (20), 4073–4082. https://doi.org/10.1021/acs.jpclett.5b01559.

(49) Yamamoto, M.; Takaki, Y.; Kashima, H.; Tsuda, M.; Tanizaki, A.; Nakamura, R.; Takai, K. In Situ Electrosynthetic Bacterial Growth Using Electricity Generated by a Deep-Sea Hydrothermal Vent. *ISME J.* **2023**, *17* (1), 12–20. https://doi.org/10.1038/s41396-022-01316-6.

(50) Barge, L. M.; Abedian, Y.; Russell, M. J.; Doloboff, I. J.; Cartwright, J. H. E.; Kidd, R. D.; Kanik, I. From Chemical Gardens to Fuel Cells: Generation of Electrical Potential and Current Across Self-Assembling Iron Mineral Membranes. *Angew. Chemie - Int. Ed.* **2015**, *54* (28), 8184–8187. https://doi.org/10.1002/anie.201501663.

(51) Kitadai, N.; Nakamura, R.; Yamamoto, M.; Takai, K.; Yoshida, N.; Oono, Y. Metals Likely Promoted Protometabolism in Early Ocean Alkaline Hydrothermal Systems. *Sci. Adv.* **2019**, *5* (6), 1–10. https://doi.org/10.1126/sciadv.aav7848.

(52) Kitadai, N.; Nakamura, R.; Yamamoto, M.; Okada, S.; Nakano, Y.; Takahashi, Y.; Takai, K.; Oono, Y. Thioester Synthesis through Geoelectrochemical. No. 2021, 1–9.

(53) Takahagi, W.; Okada, S.; Matsui, Y.; Ono, S.; Takai, K.; Takahashi, Y.; Kitadai, N. Extreme Accumulation of Ammonia on Electroreduced Mackinawite: An Abiotic Ammonia Storage Mechanism in Early Ocean Hydrothermal Systems. *Proc. Natl. Acad. Sci. U. S. A.* **2023**, *120* (41), 1–8. https://doi.org/10.1073/pnas.2303302120.

(54) Nitschke, W.; Farr, O.; Gaudu, N.; Truong, C.; Guyot, F.; Russell, M. J.; Duval, S. The Winding Road from Origin to Emergence (of Life). **2024**, 1–18.

(55) Russell, M. J. A Self-Sustaining Serpentinization Mega-Engine Feeds the Fougerite Nanoengines Implicated in the Emergence of Guided Metabolism. *Front. Microbiol.* **2023**, *14* (May). https://doi.org/10.3389/fmicb.2023.1145915.

(56) Barge, L. M.; Doloboff, I. J.; White, L. M.; Stucky, G. D.; Russell, M. J.; Kanik, I. Characterization of

Iron-Phosphate-Silicate Chemical Garden Structures. *Langmuir* **2012**, *28* (8), 3714–3721. https://doi.org/10.1021/la203727g.

(57) Hannington, M. D.; Jonasson, I. R.; Herzig, P. M.; Petersen, S. Physical and Chemical Processes of Seafloor Mineralization at Mid-Ocean Ridges; 2013; pp 115–157. https://doi.org/10.1029/GM091p0115.